

**Interaction Notes  
Note 633**

**19 November 2019**

**On the Behavior and Measurement of Electromagnetic Fields  
within an Enclosure**

**Dr. F. M. Tesche  
EMC Consultant (Retired)**

**Dr. D. V. Giri  
Pro-Tech, Wellesley, MA**

**Dept. of ECE, Univ. of New Mexico, Albuquerque, NM**

**and  
Mr. Markus Nyffeler  
armasuisse, Switzerland**

**Abstract**

*This note examines the nature of electromagnetic fields that are induced in a shielded enclosure (e.g., a cavity) by either an internal or external source. These fields are described by frequency-independent cavity modes, which when added together, provide a frequency dependent representation for the total internal field. The resulting cavity fields are seen to have a strong resonance and anti-resonance behavior, with a variation of more than 40 dB in the E-field in some cases. This large variation makes it difficult to measure the internal fields using conventional techniques that are required by MIL-STD-188-125 or IEEE 299.*

*To identify an alternative measurement procedure for such cavity fields, the existing measurement specifications are first summarized and their deficiencies for such measurements identified. Then an alternative measurement approach, based on a statistical representation of the shielding effectiveness, is suggested.*

## 1. Introduction

Ref [1] written for the Swiss NEMP Laboratory has examined a number of international standards that apply to the measurement of nuclear electromagnetic pulse (NEMP) field effects on electrical systems. Not included in [1] was a discussion of the behavior and measurement of electromagnetic (EM) fields within large shielded enclosures, like screened rooms. This is because the majority of the NEMP-related standards pertain to the testing of equipment enclosures with electrical conductors connected; investigating the behavior of large enclosures was not within the scope of [1].

With the increasing interest in higher frequency EM fields and effects, however, there is an interest in the behavior of EM fields within large enclosures. By “large”, we mean an enclosure that can measure several wavelengths, or more, on a side.

Within such enclosures, the EM field is far from simple, and many of the intuitive ideas about EM field responses that are developed from considering field sources in free space are not correct. The EM field in such enclosures is determined by an infinite set of “modes” that add together to form the total field. At certain frequencies, there are resonances in the enclosure, and the field amplitudes can become very large, and the field distribution becomes independent of the details of the excitation mechanism.

For such enclosures, measuring the internal fields is non-trivial. There can be rapid spatial variations in the fields, making the fields appear to be almost random within a finite volume. Furthermore, fixing an observation point and examining the behavior of the field as the frequency changes also produces an almost random-looking pattern in the field intensity. These observations imply that many of the existing measurement standards for lower-frequency fields are inadequate at the higher frequencies.

The purpose of this report, therefore, is to examine the nature of the EM field within cavities – using the rectangular cavity as an example – and then to review existing measurement standards relating to shielding enclosures. In the review of the measurement standards, we will find that they are *not* adequate for an accurate characterization of the internal fields, and that a new type of thinking is needed about how to describe the cavity electromagnetic field behavior.

## 2. Modal Representation of EM Fields in a Rectangular Cavity

The determination of the EM fields within a rectangular cavity has been discussed by several authors [2], [3], and [4] in terms of electric or magnetic dyadic Green's functions  $\vec{G}_e$  and  $\vec{G}_m$ , which are solutions to the vector wave equation within the cavity. The dyadic Green's function for the E-field within the cavity provides a knowledge of all three vector components for an arbitrarily oriented electric current source within the cavity, and as such, it can be used to develop an understanding of the EM fields produced by complicated wiring structures located in the cavity. In addition, similar Green's dyads can be developed for magnetic current sources, which permit the treatment of aperture sources exciting the cavity.

In this section, we will briefly examine the modal structure of the EM fields within a cavity, and will indicate the behavior of these fields as a function of position and frequency. Of course, a rectangular cavity is rather special, in that the Eigen functions (e.g., modes) for the cavity are easily determined and calculated. In a more general cavity with irregular walls and shape, these modes are difficult to determine, but nevertheless, the overall field behavior will be similar to that of the rectangular cavity.

### 2.1 Cavity Modes

The starting point for determining the EM fields within the cavity is to determine the various EM field distributions (or modes) that can exist in the cavity in the absence of any excitation. Considering the cavity of dimensions<sup>1</sup>  $a$ ,  $b$  and  $d$  as shown in Figure 1, the cavity modes are solutions to the vector wave equations

$$\nabla \times \nabla \times \vec{E} - k^2 \vec{E} = 0 \quad (1a)$$

$$\nabla \times \nabla \times \vec{H} - k^2 \vec{H} = 0, \quad (1b)$$

where  $k = \omega/c$ . These fields must also obey the boundary conditions  $\hat{n} \times \vec{E} = 0$  and  $\hat{n} \cdot \vec{H} = 0$  on the cavity walls, where  $\hat{n}$  is a vector normal to the cavity wall. Perfectly conducting cavity walls are assumed.

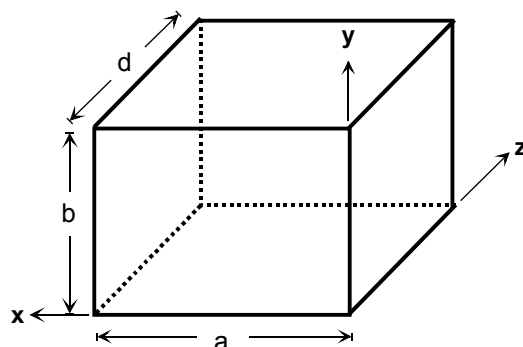


**Figure 1.** A rectangular cavity with  $(x, y, z)$  dimensions of  $a$ ,  $b$  and  $d$ .

---

<sup>1</sup> The letter  $c$  is reserved for the speed of light.

Reference [5] develops the detailed modal descriptions for the E and H fields within this cavity. This is done by dividing the fields into two general classes: fields that are transverse electric (TE to the z-direction) and transverse magnetic (TM to the z direction). This definition implies that in the TE modes, the  $E_z$  component is zero, and in the TM modes, the  $H_z$  component is zero<sup>2</sup>.

For the TE modes, all of the fields can be defined in terms of the  $H_z$  field component. For integers  $m, n = 0, 1, 2, \dots \infty$  ( $m = n = 0$  excluded), and  $p = 1, 2, \dots \infty$ , the various  $TE_{mnp}$  modes are defined in [5] as:

$$(H_z)_{mnp} = C \cos\left(\frac{m\pi x}{a}\right) \cos\left(\frac{n\pi y}{b}\right) \sin\left(\frac{p\pi z}{d}\right) \quad (2a)$$

$$(H_x)_{mnp} = -\frac{C}{k_c^2} \left(\frac{p\pi}{d}\right) \left(\frac{m\pi}{a}\right) \sin\left(\frac{m\pi x}{a}\right) \cos\left(\frac{n\pi y}{b}\right) \cos\left(\frac{p\pi z}{d}\right) \quad (2b)$$

$$(H_y)_{mnp} = -\frac{C}{k_c^2} \left(\frac{p\pi}{d}\right) \left(\frac{n\pi}{b}\right) \cos\left(\frac{m\pi x}{a}\right) \sin\left(\frac{n\pi y}{b}\right) \cos\left(\frac{p\pi z}{d}\right) \quad (2c)$$

$$(E_x)_{mnp} = \frac{j\omega\mu C}{k_c^2} \left(\frac{n\pi}{b}\right) \cos\left(\frac{m\pi x}{a}\right) \sin\left(\frac{n\pi y}{b}\right) \sin\left(\frac{p\pi z}{d}\right) \quad (2d)$$

$$(E_y)_{mnp} = -\frac{j\omega\mu C}{k_c^2} \left(\frac{m\pi}{a}\right) \sin\left(\frac{m\pi x}{a}\right) \cos\left(\frac{n\pi y}{b}\right) \sin\left(\frac{p\pi z}{d}\right) \quad (2e)$$

$$(E_z)_{mnp} = 0 \quad (2f)$$

In these expressions, C is an arbitrary constant (which will ultimately be determined by how the cavity modes are excited by some sort of a source), and

$$k_c = \sqrt{\left(\frac{m\pi}{a}\right)^2 + \left(\frac{n\pi}{b}\right)^2}. \quad (3)$$

Note that the TE cavity modes in Eq.(2) are *frequency independent* and they exist only at the resonant frequencies of the cavity, which are given as

$$f_{mnp} = \frac{c}{2} \sqrt{\left(\frac{m}{a}\right)^2 + \left(\frac{n}{b}\right)^2 + \left(\frac{p}{c}\right)^2}. \quad (4)$$

In this equation, the integers m, n and p range from 0 to  $\infty$ , with the constraint that only one integer can be zero at the time. As a result, the *minimum* resonant frequency of the

---

<sup>2</sup> The use of the z-axis is arbitrary in defining this mode structure. The x or y axis could be also chosen, and this would result in a different mode structure, but the final, total, field within the cavity would be the same.

enclosure is  $f_o = 150\sqrt{(1/L_1)^2 + (1/L_2)^2}$  (MHz), where  $L_1$  and  $L_2$  are the biggest and next to biggest of the  $(a, b, d)$  dimensions of the cavity.

Similarly, the  $TM_{mnp}$  modes are defined for  $m, n = 1, 2, \dots \infty$  and  $p = 0, 1, 2 \dots \infty$ , as

$$(E_z)_{mnp} = D \sin\left(\frac{m\pi x}{a}\right) \sin\left(\frac{n\pi y}{b}\right) \cos\left(\frac{p\pi z}{d}\right) \quad (5a)$$

$$(E_x)_{mnp} = -\frac{D}{k_c^2} \left(\frac{p\pi}{d}\right) \left(\frac{m\pi}{a}\right) \cos\left(\frac{m\pi x}{a}\right) \sin\left(\frac{n\pi y}{b}\right) \sin\left(\frac{p\pi z}{d}\right) \quad (5b)$$

$$(E_y)_{mnp} = -\frac{D}{k_c^2} \left(\frac{p\pi}{d}\right) \left(\frac{n\pi}{b}\right) \sin\left(\frac{m\pi x}{a}\right) \cos\left(\frac{n\pi y}{b}\right) \sin\left(\frac{p\pi z}{d}\right) \quad (5c)$$

$$(H_x)_{mnp} = \frac{j\omega\epsilon D}{k_c^2} \left(\frac{n\pi}{b}\right) \sin\left(\frac{m\pi x}{a}\right) \cos\left(\frac{n\pi y}{b}\right) \cos\left(\frac{p\pi z}{d}\right) \quad (5d)$$

$$(H_y)_{mnp} = -\frac{j\omega\epsilon D}{k_c^2} \left(\frac{m\pi}{a}\right) \cos\left(\frac{m\pi x}{a}\right) \sin\left(\frac{n\pi y}{b}\right) \cos\left(\frac{p\pi z}{d}\right) \quad (5e)$$

$$(H_z)_{mnp} = 0 \quad (5f)$$

Here,  $D$  is an arbitrary constant,  $k_c$  is given by Eq.(3), and again, these modes can exist only at the specific resonance frequencies given by Eq.(4).

Note that the TE and TM modes with the same indices  $m, n$ , and  $p$  have identical resonance frequencies; however, the field patterns are different. These modes are referred to as “degenerate” modes.

As an example of the mode structure for the TE and TM modes for the rectangular cavity, consider a particular cavity with dimensions  $a = 4$  m,  $b = 2$  m and  $d = 5$  m. Figure 2 presents a plot of the various resonant frequencies that exist for this cavity.

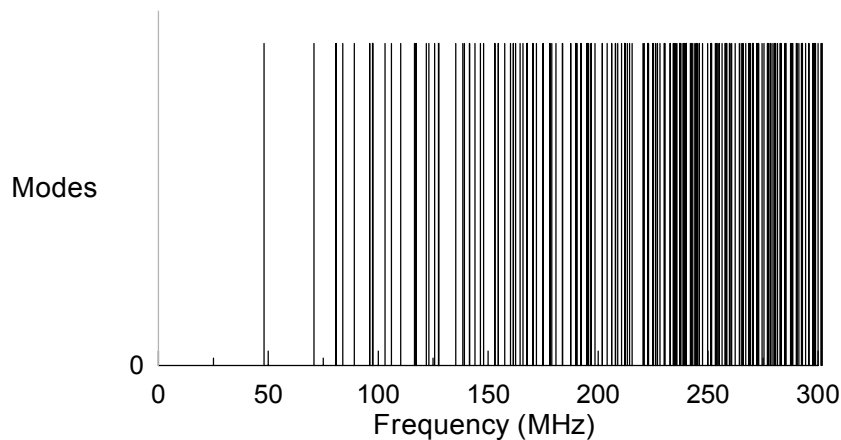


**Figure 2. Illustration of the resonant frequency structure for a rectangular cavity with dimensions  $(a, b, d) = (4, 2, 5)$  meters.**

To illustrate the spatial behavior of the modal fields, we consider the  $E_x$  field components given by Eq.(2d) and (5b) for the TE and TM modes, respectively. As shown in Figure 3, this field component is plotted in the  $x$ - $z$  plane, located at  $y = b/2$ . Removing the normalization constants, both of these fields have the following spatial dependence:

$$(E_x)_{mnp} \approx \cos\left(\frac{m\pi x}{a}\right) \sin\left(\frac{n\pi y}{b}\right) \sin\left(\frac{p\pi z}{d}\right), \quad (6)$$

and plots of this distribution for  $(m,n,p) = (0,1,1)$ ,  $(1,1,1)$  and  $(8,1,5)$  are shown in Figure 4.

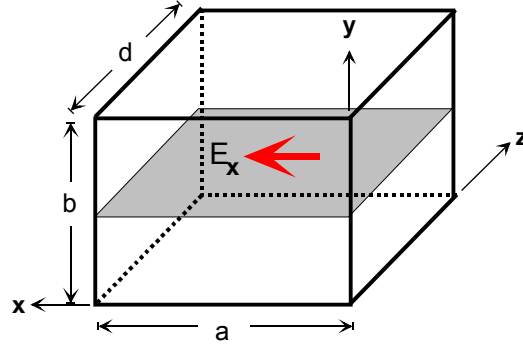


**Figure 3. Plane located at  $y = b/2$ , over which the  $E_x$  modal field components are plotted.**

In this plot we note that the mode distributions for low values of  $m$ ,  $n$  and  $p$  are slowly varying over space; however, for the higher modes, there is a rapid spatial variation. The total field within the cavity is the weighted sum of all of the modes (as determined by the excitation mechanism) and consequently, for some types of excitations there can be a rapid spatial variation of the internal fields.

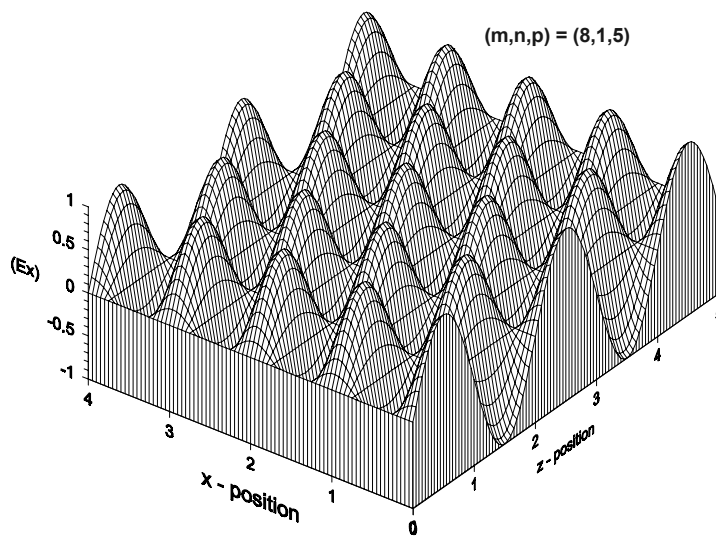
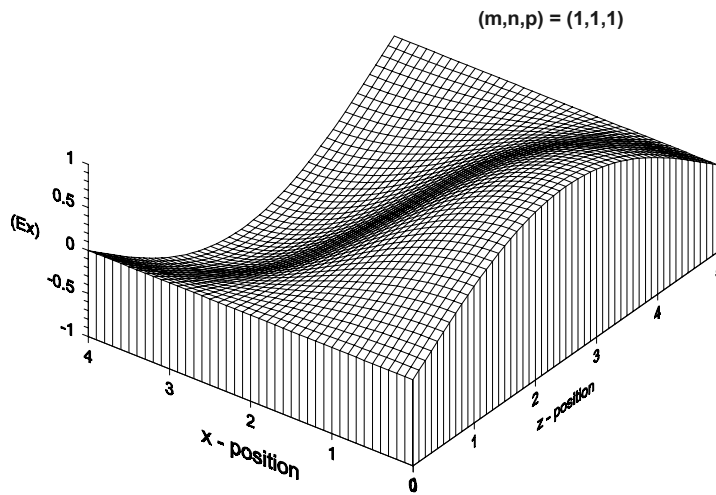
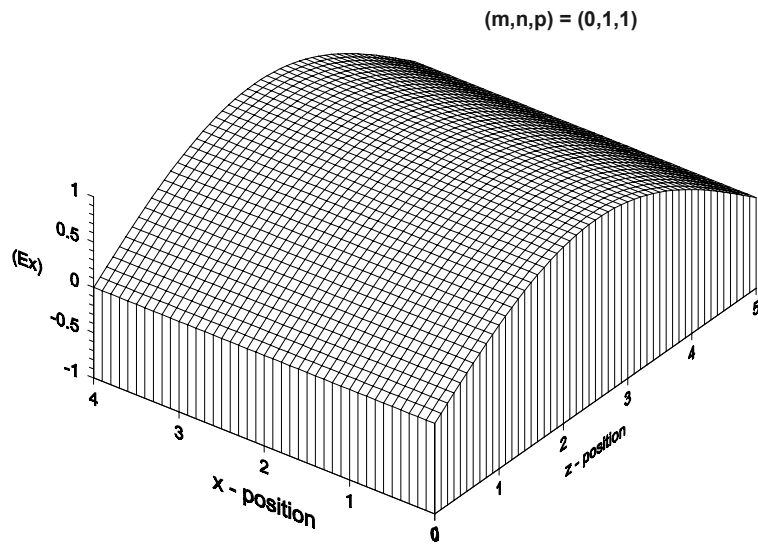


**Figure 4. Illustration of the spatial dependence of the  $(E_x)_{mnp}$  fields for both TE and TM modes for different values of the  $m$ ,  $n$  and  $p$  indices.**

## 2.2 Cavity Fields Driven by an Internal Source

With the definition of the frequency-independent cavity modes in Eqs.(2) and (5), it is possible to express the fields excited in the cavity by an internal source (antenna) or by a source on the cavity walls (aperture). While this solution is not directly applicable to the shielding problem, it does illustrate the excitation and behavior of the various cavity modes. This mode excitation is much like a Fourier series is used to represent an arbitrary function  $f(x)$  over the region  $[0,L]$  :

$$f(x) = \sum_n A_n \cos\left(\frac{n\pi x}{L}\right) + B_n \sin\left(\frac{n\pi x}{L}\right), \quad (7)$$

where  $A_n$  and  $B_n$  are suitably chosen weighting functions. For the cavity case, the sum is over three indices, and the TE and TM modes serve as the basis (or expansion) functions for the series. In this manner, we expect that the total  $E_x$  field at a location  $(x,y,z)$  will be expressible as

$$E_x(x,y,z) = \sum_m \sum_n \sum_p A_{mnp} (E_x)_{mnp}^{TE} + B_{mnp} (E_x)_{mnp}^{TM} \quad (8)$$

with similar equations (with different weighting functions) holding for the other field components. Because the TE and TM modes in Eqs.(2) and (5) are not explicit functions of frequency  $f$ , it is evident that the coefficients  $A_{mnp}$  and  $B_{mnp}$  must themselves be functions of frequency.

To illustrate the expressions for the driven E-field within the cavity, consider ref. [3], which presents a detailed derivation of the Green's functions for the rectangular cavity for the case of a  $z$ -directed current element of strength  $Idl$  located at  $r_s = (x_s, y_s, z_s)$  in a cavity having dimensions  $(a,b,d)$ . For this form of excitation, the electric field at an observation location  $r_o = (x_o, y_o, z_o)$  is given by

$$E(\vec{r}_o) = \frac{j\omega\mu}{k^2} Idl \delta(\vec{r}_o - \vec{r}_s) \hat{z} - \frac{j\omega\mu}{k^2} Idl \sum_{m=0}^{\infty} \sum_{n=0}^{\infty} \sum_{p=0}^{\infty} \left\{ \frac{\epsilon_{om} \epsilon_{on} \epsilon_{op}}{abd \left[ k^2 - \left(\frac{m\pi}{a}\right)^2 - \left(\frac{n\pi}{b}\right)^2 - \left(\frac{p\pi}{d}\right)^2 \right]} \right\} \left\{ \begin{array}{l} \left[ \left(\frac{m\pi}{a}\right)^2 + \left(\frac{n\pi}{b}\right)^2 \right] \sin \frac{m\pi x_o}{a} \sin \frac{m\pi x_s}{a} \sin \frac{n\pi y_o}{b} \sin \frac{n\pi y_s}{b} \cos \frac{p\pi z_o}{d} \cos \frac{p\pi z_s}{d} \hat{z} \\ - \left(\frac{n\pi}{b}\right) \left(\frac{p\pi}{d}\right) \sin \frac{m\pi x_o}{a} \sin \frac{m\pi x_s}{a} \cos \frac{n\pi y_o}{b} \sin \frac{n\pi y_s}{b} \sin \frac{p\pi z_o}{d} \cos \frac{p\pi z_s}{d} \hat{y} \\ - \left(\frac{m\pi}{a}\right) \left(\frac{p\pi}{d}\right) \cos \frac{m\pi x_o}{a} \sin \frac{m\pi x_s}{a} \sin \frac{n\pi y_o}{b} \sin \frac{n\pi y_s}{b} \sin \frac{p\pi z_o}{d} \cos \frac{p\pi z_s}{d} \hat{x} \end{array} \right\} \quad (9)$$

In this expression, the term  $\epsilon_{om} = 1$  for  $m = 0$ , and  $= 2$  for  $m \neq 0$ , etc. The first term containing the  $\delta$ -function is required only when the field is evaluated within the source region. For our purposes, we will be evaluating the fields away from the source, so only the

triple sum term will be required. A similar expression can be developed for the Green's function for the magnetic field using the approach reported in [3].

Although the expression in Eq.(9) gives an explicit equation for the E-field, it is computationally unwieldy, due to the very slow convergence of the sums. Reference [4] has studied the convergence of this series and reports needing  $\approx 90,000$  terms in the series in some cases. An alternative to a brute force summation of the entire series is to use the summation formulas [6]

$$\sum_1^{\infty} \frac{\cos nx}{n^2 - a^2} = \frac{1}{2a^2} - \frac{\pi \cos(x - \pi)a}{2a \sin \pi a} \quad \text{for } 0 \leq x \leq 2\pi \quad (10a)$$

$$\sum_1^{\infty} \frac{n \sin nx}{n^2 - a^2} = \frac{\pi \sin(\pi - x)a}{2 \sin \pi a} \quad \text{for } 0 \leq x \leq 2\pi \quad (10b)$$

to reduce the sums to 2-dimensional series. Equation (10a) may be applied to the  $\hat{z}$  component, and Eq.(10b) may be applied to the  $\hat{y}$  and  $\hat{x}$  terms of Eq.(9). In doing this the expressions for the  $E_z$  field component becomes

$$E_z(x_o, y_o, z_o) = \frac{-j\omega\mu Idl}{k^2(abd)} \sum_{m=0}^{\infty} \sum_{n=0}^{\infty} \Gamma_{mn} \left( \frac{d}{2k'} \right) \frac{\cos k'(z_o + z_s - d) + \cos k'(|z_o - z_s| - d)}{\sin k'd} \quad (11a)$$

with

$$\Gamma_{mn} = \epsilon_{om} \epsilon_{on} \left( \left( \frac{m\pi}{a} \right)^2 + \left( \frac{n\pi}{b} \right)^2 \right) \sin \frac{m\pi x_o}{a} \sin \frac{m\pi x_s}{a} \sin \frac{n\pi y_o}{b} \sin \frac{n\pi y_s}{b}. \quad (11b)$$

Similarly, the  $E_y$  field is given as

$$E_y(x_o, y_o, z_o) = \frac{-j\omega\mu Idl}{k^2(abd)} \sum_{m=0}^{\infty} \sum_{n=0}^{\infty} \Gamma'_{mn} \left( \frac{d}{2} \right) \frac{\sin k'(d - (z_o + z_s)) + \text{sgn}(z_o - z_s) \sin k'(d - |z_o - z_s|)}{\sin k'd} \quad (12a)$$

with

$$\Gamma'_{mn} = \epsilon_{om} \epsilon_{on} \left( \frac{n\pi}{b} \right) \sin \frac{m\pi x_o}{a} \sin \frac{m\pi x_s}{a} \cos \frac{n\pi y_o}{b} \sin \frac{n\pi y_s}{b}, \quad (12b)$$

and the  $E_x$  field is

$$E_x(x_o, y_o, z_o) = \frac{-j\omega\mu Idl}{k^2(abd)} \sum_{m=0}^{\infty} \sum_{n=0}^{\infty} \Gamma''_{mn} \left( \frac{d}{2} \right) \frac{\sin k'(d - (z_o + z_s)) + \text{sgn}(z_o - z_s) \sin k'(d - |z_o - z_s|)}{\sin k'd} \quad (13a)$$

with

$$\Gamma''_{mn} = \epsilon_{om} \epsilon_{on} \left( \frac{m\pi}{a} \right) \cos \frac{m\pi x_o}{a} \sin \frac{m\pi x_s}{a} \sin \frac{n\pi y_o}{b} \sin \frac{n\pi y_s}{b}. \quad (13b)$$

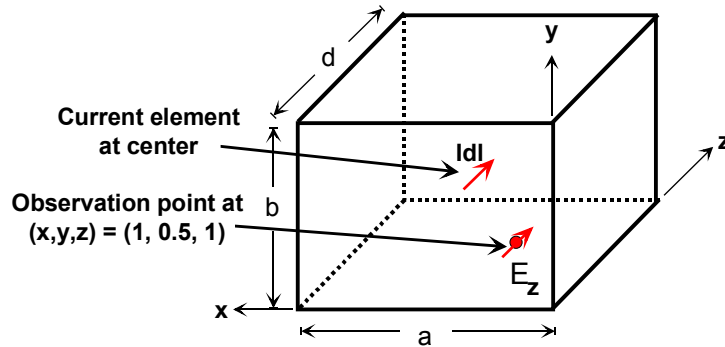
In these expressions, the term  $k'$  is defined as

$$k' = \sqrt{k^2 - \left(\frac{m\pi}{a}\right)^2 - \left(\frac{n\pi}{b}\right)^2} \quad (14)$$

with  $k = \omega/c$ . Note that the field expressions in Eqs.(11 – 13) contain a frequency dependence through the  $k$  and  $k'$  terms, and consequently, an excitation at any frequency will provide a response for the internal fields, even though the modes are defined only at the discrete frequencies given by Eq.(4). Also notice that there are resonances in this response occurring at frequencies corresponding to the zeros  $\sin(k'd)$  in the denominator of Eqs.(11 – 13), and these correspond to the resonances of Eq.(4). Because there is no loss in this idealized problem, the responses at these resonance frequencies are infinite

For small values of the indices  $m$  and  $n$  the value of  $k'$  is real if  $k^2 > (m\pi/a)^2 + (n\pi/b)^2$ . However, as  $m$  and  $n$  increase, the value of  $k'$  eventually becomes imaginary and the sine and cosine terms in Eqs.(11 – 13) become exponentially damped, and the series begins to converge very rapidly. Consequently, for low frequencies, the series in Eqs.(11 – 13) are very efficient for evaluating the cavity fields.

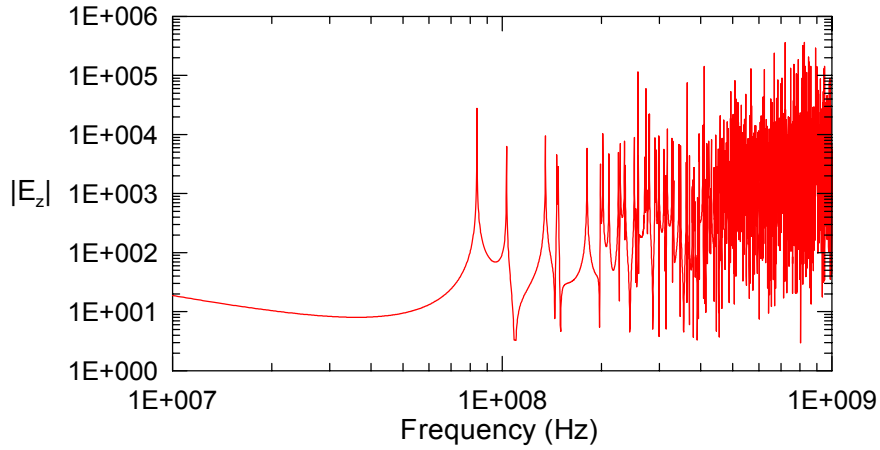
To illustrate the calculation of the cavity fields using Eqs.(11 – 13) consider again the cavity with the dimensions  $(a, b, d) = (4, 2, 5)$  m with a time-harmonic,  $z$ -directed electric current element with  $Idl = 1$ , located at the cavity center  $(x_s, y_s, z_s) = (2, 1, 2.5)$  m. The geometry of this source configuration is shown in Figure 5.



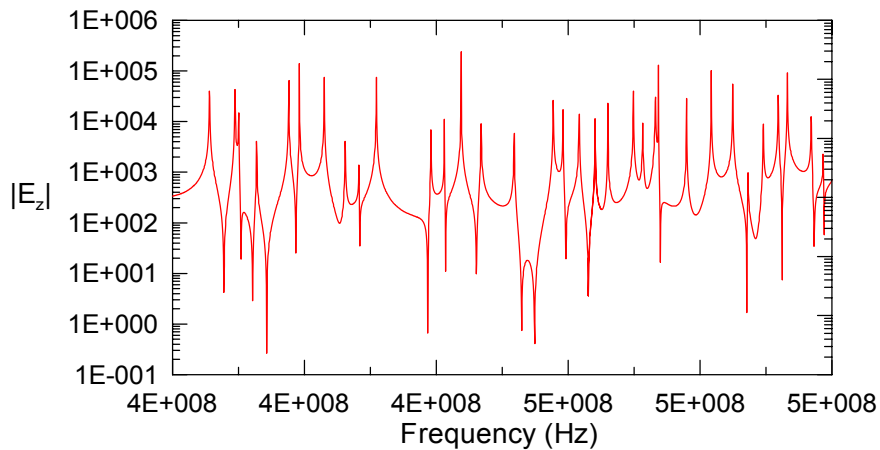
**Figure 5. Illustration of a  $z$ -directed current element at the center of the rectangular cavity, and a field observation point.**

Figure 6 shows the spectrum of the  $E_z$  field component at the observation point  $(x_o, y_o, z_o) = (1, 0.5, 1)$  m. The other E-field and H-field components have a similar behavior. At low frequencies, the field behavior is rather smooth, but as the frequency increases, the various cavity resonances cause rapid flections of the field intensity (over 5 orders of magnitude) as the frequency changes slightly.

Focusing on a narrow portion of the frequency range, Figure 7 shows the spectrum swept from 400 to 500 MHz. Clearly, there is a very large variation of the E-field intensity as the frequency changes.



**Figure 6.** Frequency domain spectrum of the  $E_z$  field at  $(x_o, y_o, z_o) = (1, 0.5, 1)$  m produced by a  $z$ -directed current element with strength  $Idl = 1$  at  $(x_s, y_s, z_s) = (2, 1, 2.5)$  m in a rectangular box enclosure.

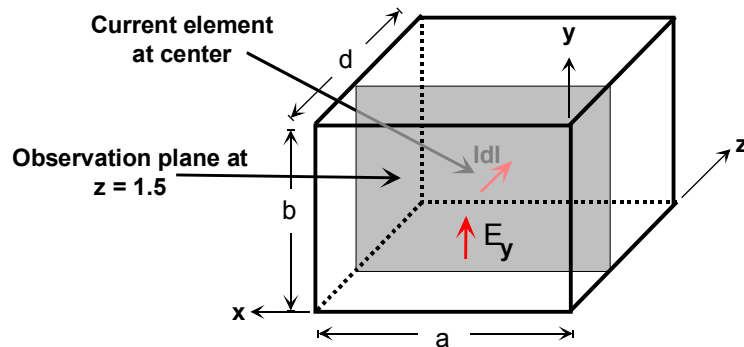


**Figure 7.** Frequency domain spectrum of the  $E_z$  field for the same source and observation conditions as in Figure 6, swept from 400 to 500 MHz.

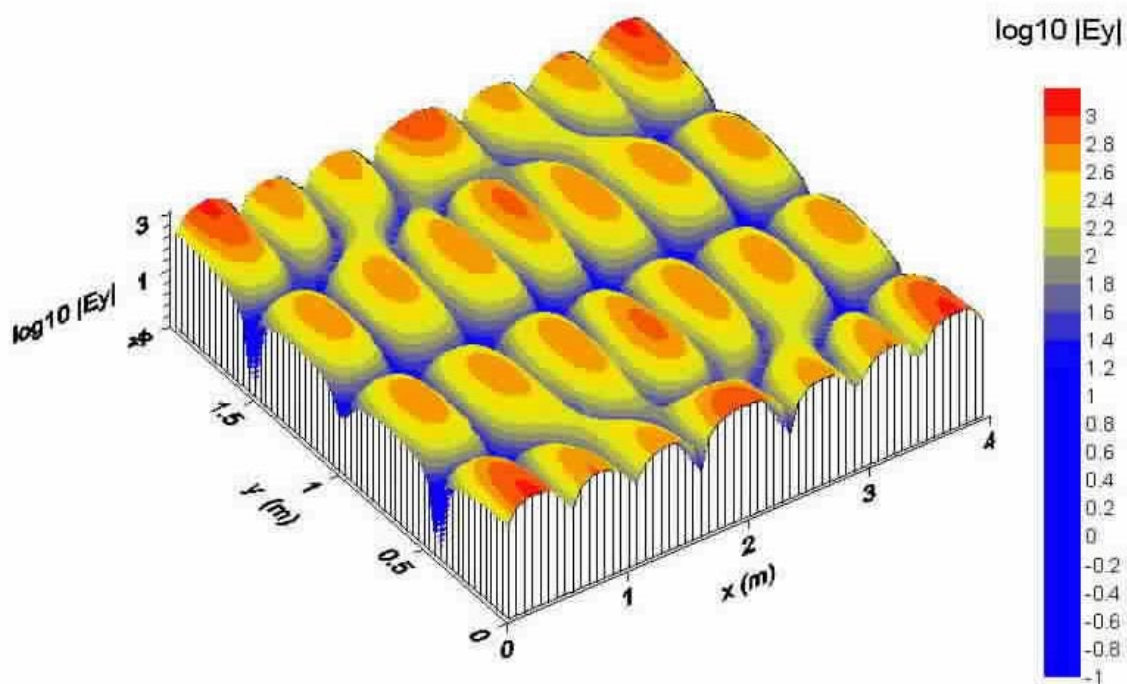
Similar variations in the E-field intensity are noted as the observation location within the cavity is changed. To illustrate this attribute of the cavity field environment, the  $E_y$  field component is plotted over an  $x$ - $y$  observation plane located at  $z = 1.5$  m. As before, this cavity field is produced by a  $z$ -directed unit amplitude current element ( $Idl = 1$ ) located at the center of the cavity.

Figure 9 illustrates the surface plot of the log-magnitude of the  $E_y$  field component over the  $z = 1.5$  m plane at a frequency of 500 MHz for the  $z$ -directed current element. As before, there is a 5 order of magnitude variation of the field intensity over this observation plane. This fact, together with the observations of the frequency variations of Figure 6, suggest that any sort of useful descriptor of the EM field behavior within the cavity should, in some way, involve either a spatial or a frequency domain average, so as to eliminate the

very large variations in the response quantity. This suggests that some sort of a statistical description of the fields may be useful. This subject is explored further in the next section.



**Figure 8.** Illustration of the rectangular cavity of Figure 1 with an  $x$ - $y$  observation plane at  $z = 1.5$  m, over which the  $E_y$  field component produced by the  $z$ -directed current element  $Idl$  is plotted.



**Figure 9.** Surface plot of the log-magnitude of the  $E_y$  field component in the  $z = 1.5$  m plane at a frequency of 500 MHz for the  $z$ -directed current element with strength  $Idl = 1$  and located at  $(x_s, y_s, z_s) = (2, 1, 2.5)$  m in a rectangular box enclosure.

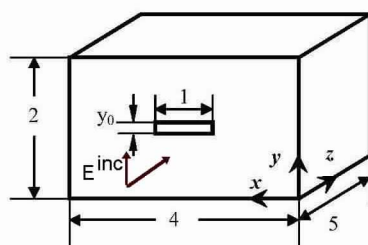
### 2.3 Cavity Fields Excited by an External Source

The problem of EM shielding by an enclosure with an aperture can be described by a modal analysis similar to that of the dipole excitation of the cavity treated in the previous section. As noted in Figure 10, an incident EM field is polarized in the  $y$ -direction and is normally incident on a rectangular aperture in the cavity. In this shielding study, the cavity will have the same dimensions  $(a, b, d) = (4, 2, 5)$  m as for the cavity shown in Figure 1.

The incident EM field striking the enclosure penetrates through the aperture, and once within the cavity, it excites the internal cavity modes, much like the dipole source discussed in the previous section. The resulting internal field distribution thus can be described as a sum over the TE and TM modes as in Eq.(8), with the modal coefficients being determined from a knowledge of the aperture E-field distribution.

Unfortunately, the aperture E-field distribution is not known a-priori, and it must be determined from a solution of the coupled interior and exterior EM interaction problem. As described in [7], there are several different approaches for determining the aperture E-field distribution and the resulting internal cavity field. These include the integral equation (IE) method, the finite-difference time domain (FDTD) method, and the multilevel fast multipole algorithm (MLFMM).

Reference [8] has analyzed the cavity fields for the geometry shown in Figure 10 using the moment method, and has presented a comprehensive study of the behavior of the internal field distribution<sup>3</sup>. In this section of the report, we will illustrate and summarize the results of this reference, many of which are dictated by the internal cavity mode structure.



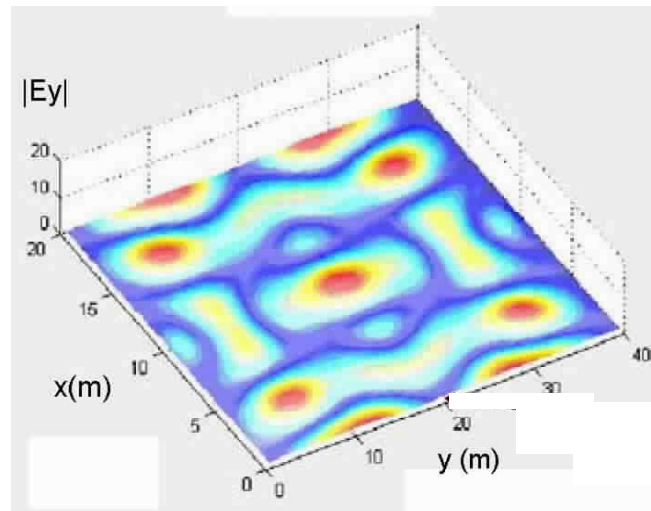
**Figure 10.** The rectangular cavity of Figure 1 with a narrow aperture of length 1 m centered in the  $x$ - $y$  plane at  $z = 0$ , and illuminated by a normally incident,  $y$ -polarized E-field.

Figure 11 presents a surface plot of the magnitude of the  $E_y$  field component in the  $x$ - $y$  plane located at  $z = 2.5$  m in the cavity of Figure 12 at a frequency of 500 MHz. In this plot, it is apparent that there are a number of “hot spots” in the cavity fields – well away from the aperture, where the field is large. It is interesting to note that the field in this aperture excitation case does not have as many peaks and valleys, as does the field in

---

<sup>3</sup> Actually, reference [8] treats a cavity that is a factor of 10 smaller than what is considered here, namely one with dimensions  $(a, b, d) = (40, 20, 50)$  cm. Their calculated results have been scaled down in frequency by a factor of 10 to be compatible with the larger cavity that we are considering in this report.

Figure 9, which is due to the internal source. This is because many of the cavity modes are not excited by the E-field source (magnetic current) located on the cavity wall.



**Figure 11. Surface plot of the  $E_y$  field magnitude in the  $x$ - $y$  plane located at  $z = 2.5$  m (middle) for the cavity of Figure 12.**

Figure 12 presents the computed E-field shielding effectiveness of this cavity with aperture over a frequency range of 400 to 500 MHz. In this case, the calculation was for the  $y$ -component of the internal E-field near the center of the cavity, as reported by ref. [8].

When this plot is compared with the spectrum plot for the internal source in Figure 7, we note a similar behavior, although there are more resonances and anti-resonances for the internal source spectrum for reasons stated earlier. Furthermore, it is apparent that the data in Figure 12 is not sampled finely enough in frequency to generate the detail found in the spectrum of Figure 7.

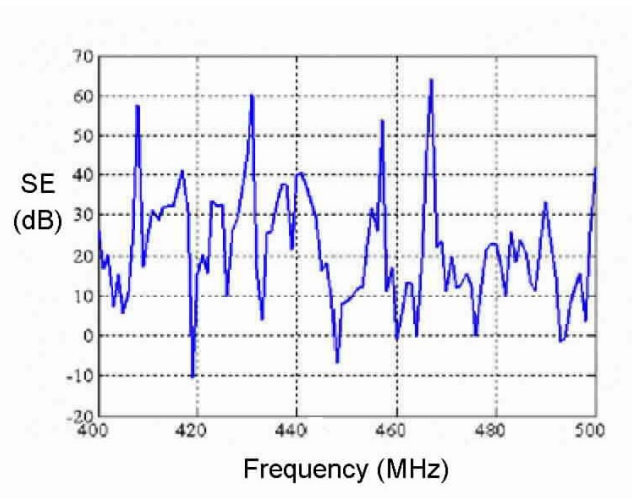


**Figure 12. Plot of the computed shielding effectiveness (in dB) for the  $y$ -component of the internal E-field near the center of the cavity over a frequency range of 400 to 500 MHz (from ref [8].)**

Reference [8] makes an interesting observation that the behavior of the field variation in Figure 12 looks almost random, and in fact, it could be described by statistical methods. For example, by computing the shielding effectiveness figure for the  $E_y$  field component at 100 random points in the cavity over a frequency range of 400 to 500 MHz, the various overlay plots of the variations of these calculations is shown in Figure 13. By binning the SE values for each of these traces and computing a cumulative probability distribution (CPD), the family of probability curves of Figure 14 results.

Figure 15 presents a close-up plot of the bottom portion of the cumulative probability curve of Figure 14, illustrating a finite probability of having field enhancement (a negative shielding effectiveness) within the cavity.

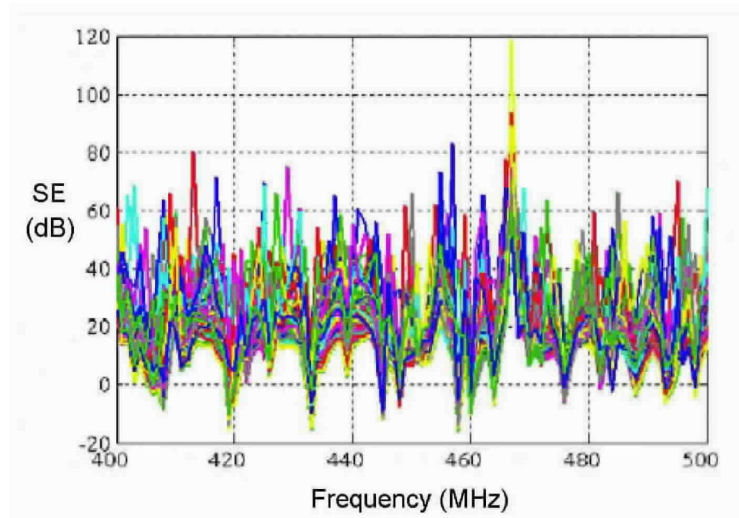


**Figure 13.** Overlay plots of the shielding effectiveness for  $E_y$  at 100 random points in the cavity, over a frequency range of 400 to 500 MHz (from ref [8].)

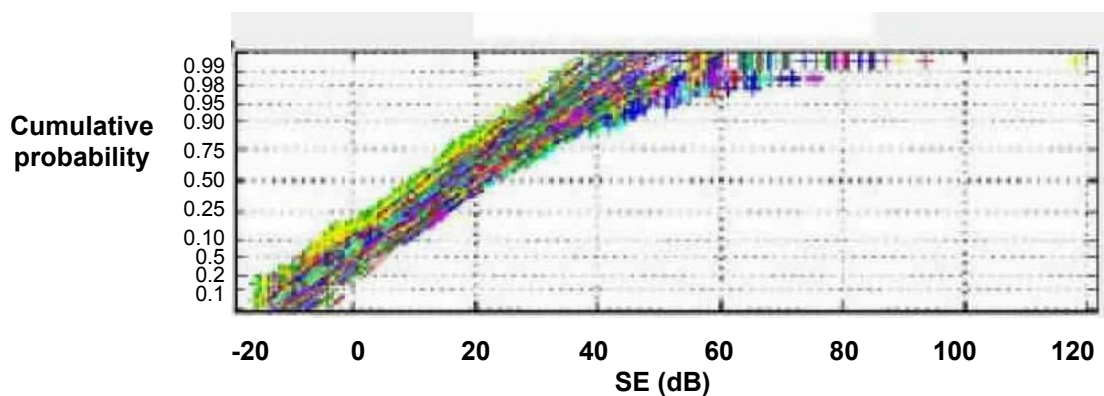


**Figure 14.** Cumulative probability distributions for the shielding effectiveness of the  $E_y$  field component, using the data for the 100 observation points shown in Figure 13 (from ref [8].)

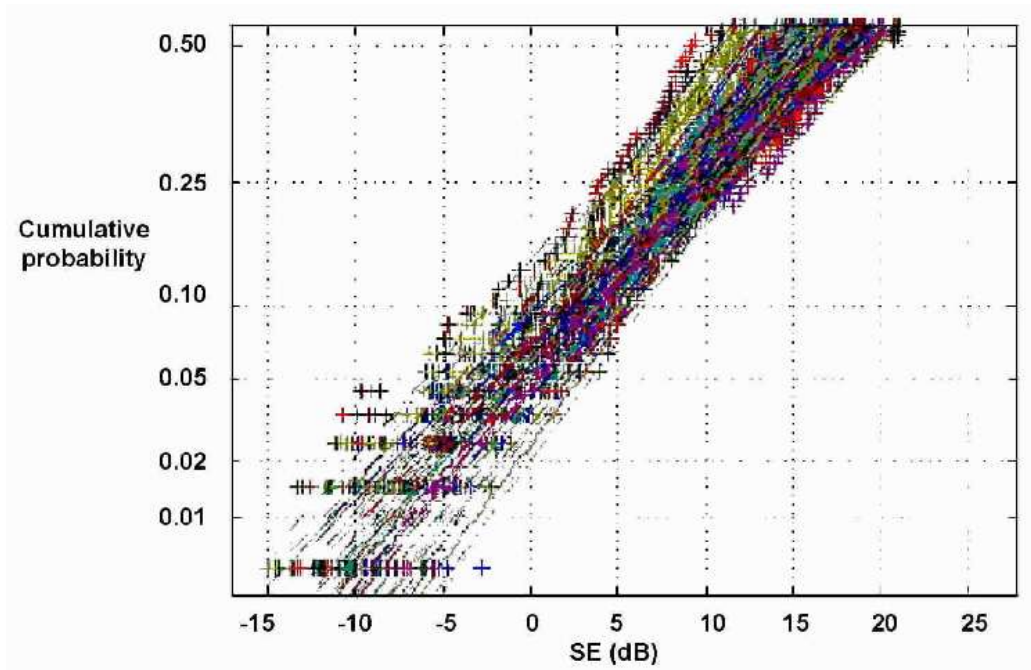


**Figure 15.** Close-up of the bottom portion of the cumulative probability curve of Figure 14, illustrating a finite probability of having field enhancement (a negative shielding effectiveness) within the cavity.

#### ***2.4 Statistical Representations of Cavity Fields***

The argument that statistical tools are appropriate for describing the fields in resonant cavities has also been made by ref. [9], where it is argued that the field behavior in a cavity can be described by the same statistical distribution function that is used in a mode-stirred chamber. In this paper, the authors show that the coupling between a sensor in an electrically large metallic cavity and the outside world is a very complicated problem, with small changes inside the cavity resulting in signal changes of greater than 20 dB. However, they show that this problem can be greatly simplified by separating the task into two components: a statistical “reverberation chamber” type component, and a deterministic component (giving trends as a function of aspect angle, frequency, or other parameters). They give appropriate methods for evaluating each of these effects, and show how they can be applied to specific problems.

### **3. Standard Measurements of Enclosure Shielding**

The discussions in the preceding section have illustrated that the EM field distribution within a shielded enclosure can be very complex – especially at high frequencies, where the field is composed of many resonant modes. Furthermore, determining the proper way of making meaningful measurements in such cavities is difficult to do.

There are several standards that have been developed to try to provide “simple” measurement procedures for performing such measurements. Two of the more common standards are the IEEE STD 299, and the MIL-STD-188-125. In this section, these and other international standards are reviewed, and their applicability to the understanding the behavior of the shielding in cavities is examined.

#### **3.1 IEEE STD 299-1997**

##### *3.1.1 Overview*

The IEEE 299 Standard [10] provides uniform measurement procedures and techniques for determining the effectiveness of electromagnetic shielding enclosures at frequencies from 9 kHz to 18 GHz (extendable to 50Hz and 100 GHz, respectively) for enclosures having no dimension smaller than 2.0 m. The types of enclosures covered include, but are not limited to, single-shield or double-shield structures of various constructions, such as bolted demountable, welded, or integral with a building, and made of materials such as steel plate, copper or aluminum sheet, screening, hardware cloth, metal foil, or shielding fabrics.

In this standard, the shielding effectiveness (SE) is defined as the ratio of the signal received (from a transmitter) without the shield, to the signal received inside the shield; the insertion loss when the shield is placed between the transmitting antenna and the receiving antenna (IEEE Std 100-1996). Depending on the frequency range of the measurement, the “signal” can be either the electric (E) field or the magnetic (H) field, and these observables are defined in the document.

The present report is not meant to provide a detailed description of the IEEE 299 Standard, but rather, serves to examine this standard and its recommended measurement procedures from the viewpoint of wanting to make accurate, wide-band shielding measurements useful for understanding the behavior of transient EM fields within enclosures. For specific information about the IEEE 299 measurement requirements, please consult with the original document.

##### *3.1.2 Measurement Concepts*

The following section describes general measurement concepts for making the shielding effective measurements using the IEEE 299 method.

### 3.1.2.1 Measurement Frequencies and Antennas

The IEEE 299 Standard defines three different frequency ranges in which the measurements must be made. These are listed in Table 1, and are in a “low” frequency range, a “resonant” frequency range, and a “high” frequency range. Due to the nature of EM radiation from antennas over wide frequency ranges, different types of antennas are specified over the various frequency ranges, and these also are indicated in the table.

**Table 1. Definition of the IEEE 299 measurement frequency ranges and the required transmitting antennas for exciting the enclosure.**

Standard Frequency	Antenna Type	Clause Reference
Low range <sup>a</sup>		
9 – 16 kHz	Small loop	5.6
140 – 160 kHz	Small loop	5.6
14 – 16 MHz	Small loop	5.6
Resonant range <sup>a</sup>		
20 – 100 MHz	Biconical antenna	5.7
100 – 300 MHz	Dipole antenna	5.7
High range <sup>b</sup>		
0.3 – 0.6 GHz	Dipole antenna	5.7
0.6 – 1.0 GHz	Dipole antenna	5.7
1.0 – 2.0 GHz	Horn antenna	5.7
2.0 – 4.0 GHz	Horn antenna	5.7
4.0 – 8.0 GHz	Horn antenna	5.7
8.0 – 18.0 GHz	Horn antenna	5.7

a. Actual test frequencies should be according to the test plan

b. A single frequency in each band is recommended, but actual test frequencies should be according to the test plan.

### 3.1.2.2 Measured Response Quantities

The standard also defines the quantities to be measured in each of the frequency ranges of Table 1. Specifically, in the low frequency range of 9 kHz to 20 MHz, the measurements are to be of the magnetic (H) field, or equivalently, of the voltage outputs from magnetic field sensors. In the resonant range of 20 MHz to 300 MHz, the electric (E) field is to be measured, and for the high frequency range of from 1.7 to 18 GHz, the measurement is to be of the power received by the horn antenna due to the received electromagnetic field. (Note that these frequency ranges, as provided in Table 3 of the IEEE 299 specification, are not consistent with those of Table 1 above and the corresponding Table 1 of the standard.)

With these measured field quantities, the shielding effectiveness of the enclosure is defined as follows:

$$SE_H = 20 \log \left( \frac{H_{ref}}{H_{in}} \right) \quad (dB) \quad (\text{for magnetic field}) \quad (15a)$$

$$SE_E = 20 \log \left( \frac{E_{ref}}{E_{in}} \right) \quad (dB) \quad (\text{for electric field}) \quad (15b)$$

$$SE_P = 10 \log \left( \frac{P_{ref}}{P_{in}} \right) \quad (dB) \quad (\text{for power}) \quad (15c)$$

In these expressions, the subscript “ref” refers to the reference field (or power) quantity, which according to the definition in the 299 Standard is the signal received from the transmitter without the shield present (e.g., the “incident” signal). Similarly, the subscript “in” refers to the signal received inside the shield, which is attenuated by the presence of the shield.

### 3.1.3 Measurement Procedures

Different procedures are required for each of the three frequency ranges of Table 1. These are reviewed below.

#### 3.1.3.1 Low-frequency measurements (9 kHz to 20 MHz)

The low-frequency measurements of the IEEE 299 Standard utilize a small electrostatically shielded loop of diameter 0.3 m. Because of its size, this enables evaluation of the performance of the enclosure when exposed to magnetic sources near the enclosure walls.

The locations of the transmitting and receiving loops, relative to the shield wall, are shown in Figure 16. As noted in the standard, the transmitting and receiving loops are to be set-up away from the shield, but with the same separation between the two loops, and the reference field  $H_{ref}$  measured. Then, the loops are to be placed a distance of 0.3 meters on each side of the shield wall, and the measurement of the H-field within the shielded region made.

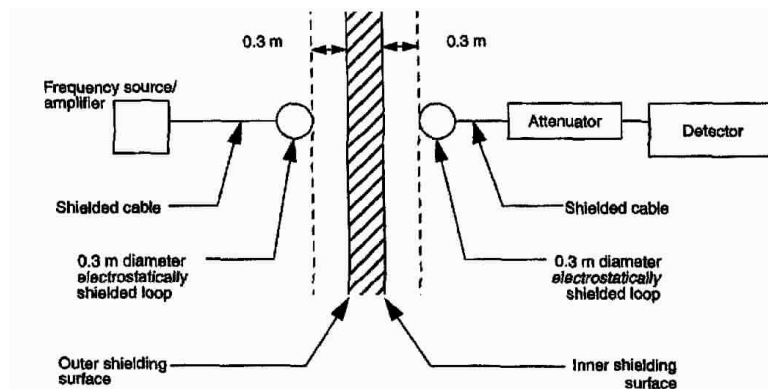


**Figure 16. Schematic diagram of the test configuration for magnetic field tests, showing the dimensions of the transmit and receive antennas. (Taken from [10].)**

The low frequency magnetic field measurements are to be made in accordance with Figure 16, with the transmitting and receiving loops each spaced by 0.3 m from the respective shielding barrier and coplanar in a plane perpendicular to the wall, ceiling, or other surface being measured.

During these low-frequency measurements, one loop (typically the transmit loop) is maintained in a fixed position and the second loop (typically the receive loop) is reoriented and moved within the shielded region to determine the worst-case measurement (i.e., the largest internal H-field). This maximum indication of the detector reading is used for determining the calculation of the magnetic field SE using Eq.(15).

### *3.1.3.2 Resonant range measurements (20 MHz to 300 MHz)*

The resonant range procedure directly measures the effect of electromagnetic sources at positions over all accessible surfaces of the enclosure. It is known that impinging fields may not be planar, especially in the lower portions of the range. It is further recognized that the general geometric shape and physical size of the shielded enclosure can significantly affect measurements

Since the majority of enclosures that are expected to be tested will have their fundamental resonance point in this range, it is noted that that very large internal field responses can be observed at these frequencies. The IEEE 299 Standard states that “all reasonable attempts should be made to avoid testing at, or very near, the enclosure resonant frequency”. Such resonance frequencies for a rectangular cavity are given by Eq.(4). However, there are enclosure systems that are specified by their owners to provide a level of performance in this frequency range due to the anticipated usage, or other factors, and that must be tested in this range regardless of potential resonance effects. Thus, the testing should be performed at a frequency or frequencies determined by the owner and incorporated in the approved test plan.

The setup for measuring the reference field for the resonance region measurements is shown in Figure 17. The electromagnetic fields are to be generated by a biconical antenna for frequencies in the range of 20 MHz to 100 MHz, and by to a  $1/2 \lambda$  dipole for frequencies at or above 100 MHz.

The receiving antenna is supposed to be the same type used for transmitting. When the dipole antenna is used, it is also to be  $1/2 \lambda$  in length, and its output is to be through a balun transformer and coaxial cable to the field-strength measuring device (typically a spectrum analyzer.) The antenna feed cable is to be aligned perpendicular to the axis of the antenna for a distance of at least 1 m, and it is to employ either continuous loaded ferrite jacketing or ferrite beads located at the ends and midpoint of the cable. Shown in this figure are the transmitting and receiving antennas in the horizontal orientation. The orthogonal (vertical) antenna positions are also to be considered in these reference field measurements, as described below.

To determine the reference field with a horizontal antenna orientation for both antennas (of either type), the receive antenna is to be moved vertically at least  $\pm 0.5$  m from the initial position. With vertical orientation for both antennas (of either type), the receive antenna is to be moved laterally at least  $\pm 0.5$  m from the initial position. For any fixed

antenna position, the maximum field strength reading is noted, and this determines the reference E-field level.

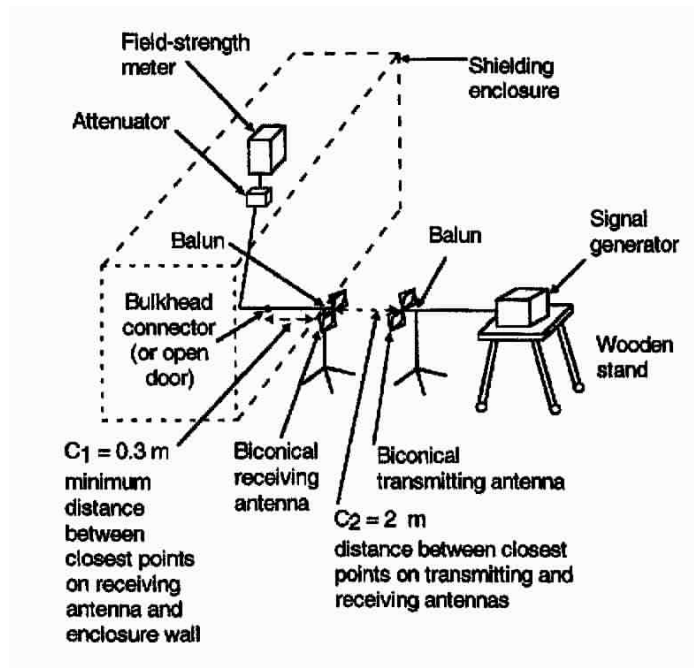


**Figure 17. Illustration of the transmitter and receiver antenna locations for measurement of the reference E-field in the resonance range of 20 MHz to 300 MHz.**

For the measurement of the internal E-field, and hence, the determination of the E-field SE, the receive antenna is located inside the shielded enclosure, and then its position and polarization are swept throughout the shield interior in a manner prescribed by the IEEE 299 Standard. This procedure is illustrated in Figure 18. This sweeping is done to obtain the largest detector response, and this is used with Eq.(15) to determine the worst-case (smallest) E-field shielding effectiveness.

It is important to note that the above test procedure is to be repeated for all external transmitter locations (which are either specified in the IEEE 299 Standard, or in a test-specific test plan), as well as for all frequencies specified in the resonance region frequency band.

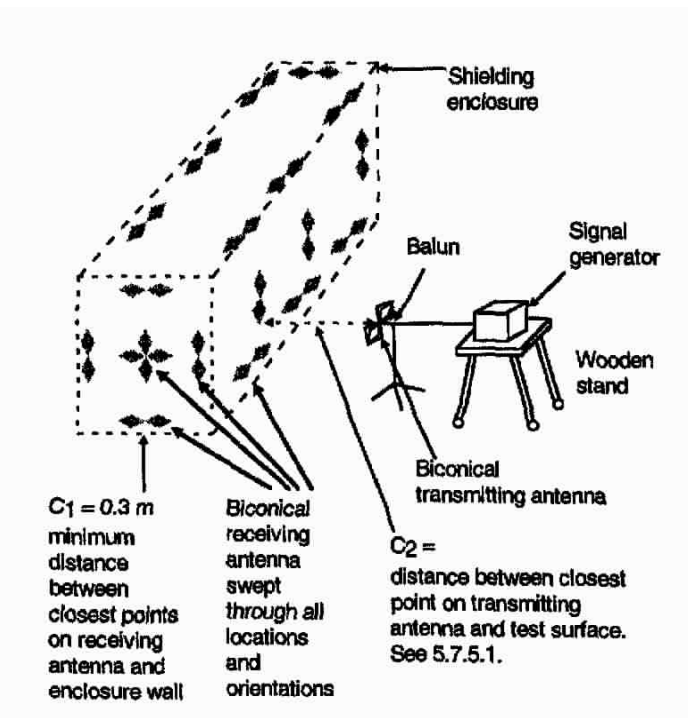


**Figure 18. Illustration of the measurement of the internal E-field in the resonance region, achieved by sweeping the internal antenna in position and polarization within the enclosure.**

### 3.1.3.3 High-frequency measurements (300 MHz to 18 GHz)

The high-frequency test procedure directly measures the effect of radiating sources at positions over all accessible surfaces of the enclosure. The fields impinging on the shield are to as planar as the relative wavelength and surrounding structure allows.

For shielding measurement testing in this range, the recommended frequencies are a single frequency within each of the following bands: 300MHz to 600 MHz; 600 MHz to 1GHz; 1 – 2 GHz; 2 –4 GHz; 4 –8 GHz; and 8 – 18 GHz. Actual test frequencies, however, are to be selected by the owner of the test facility, and in accordance with the test plan. In all cases, the lowest test frequency in this procedure should be at least three times the lowest cavity resonant frequency, as determined by from Eq.(4).

The testing procedure in this frequency range is similar to that in the resonance band, in that first a reference E-field is measured and then the E-field component within the shielded enclosure is measured and the SE calculated. As in the previous case, this section of the IEEE 299 Standard also specifies that the transmitter location and the internal antenna (receiver) location be swept through specified positions and polarizations at each measurement frequency to ascertain the *maximum* internal E-field (and hence the minimum shielding effectiveness).

The equipment set-up for determining the reference field depends on the frequency range of the measurements, as shown in Figure 19. For frequencies less than 1 GHz, the reference (receiving) antenna is located outside the enclosure, at a distance  $d$  from the enclosure wall, as shown in part a of the figure. This value of  $d$  is to be at least 0.3 m and its value is adjusted to  $\lambda/4$ , where there is a maximum in the measured response of the

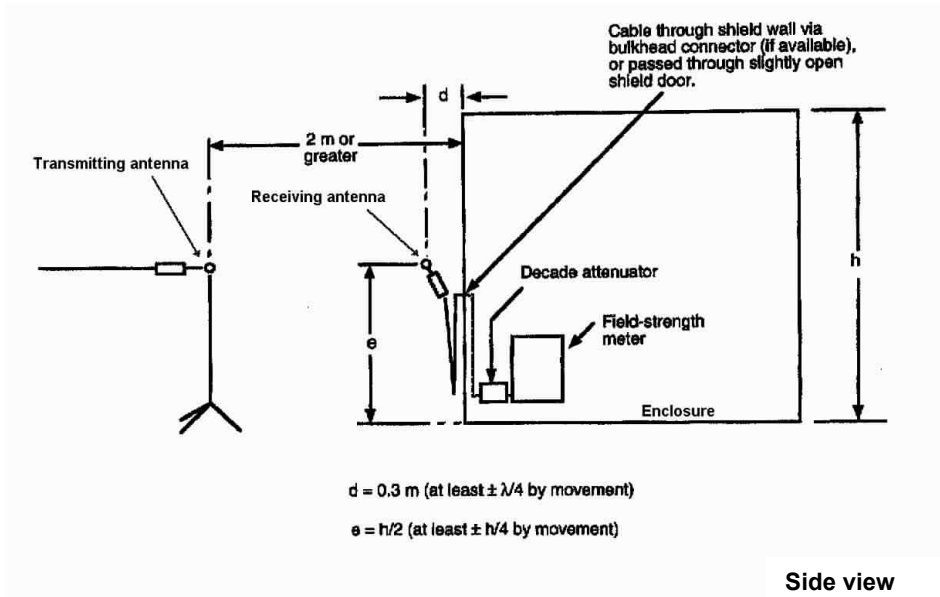
reference antenna. Thus, as in the case of the reference field for the resonance region, the maximum E-field outside the enclosure is used for the reference.

For frequencies greater than 1 GHz, the horn type antennas are used, as shown in Figure 19b and the reference fields are measured away from the enclosure, much like the reference field measurement for the low-frequency loop antennas. This yields a reference field that is the true incident field.

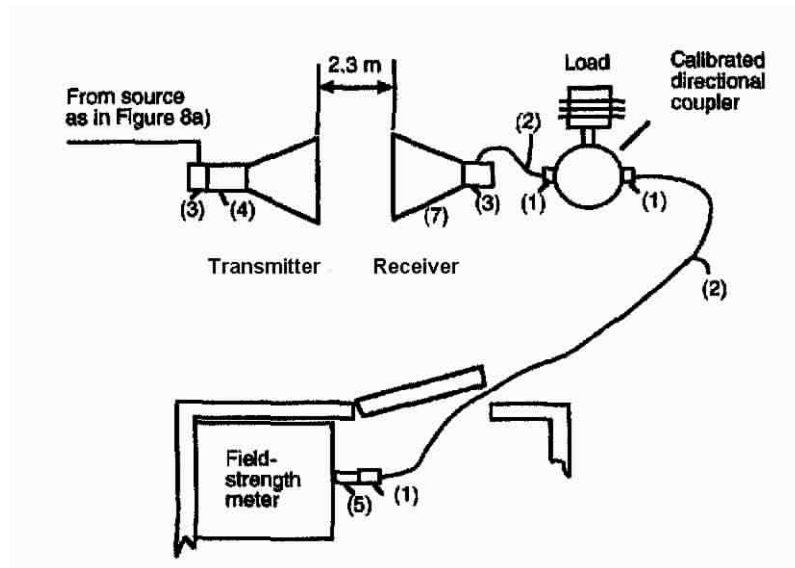
The IEEE 299 Standard provides a considerable amount of information regarding the interconnection of the measurement equipment and the procedures for making these measurements, which are beyond the scope of this present discussion. The interested reader is referred to this document for more information.

The setups for the high frequency measurements are shown in Figure 20 for the cases of  $f < 1$  GHz and  $f > 1$  GHz in parts *a* and *b*, respectively. Basically, the test procedure is similar to that of the resonance region measurement. For the measurement of the internal E-field the receive antenna is located inside the shielded enclosure and its position and polarization are swept throughout the shield interior in a manner prescribed by the IEEE 299 Standard. This sweeping determined the largest detector response, and it is used with Eqs.(15) to determine the worst-case shielding effectiveness.

As before, this test procedure is repeated for all external transmitter locations (which are either specified in the IEEE 299 Standard, or in a test-specific test plan), as well as for all frequencies specified in the frequency band.



**a. Frequencies < 1 GHz**



**b. Frequencies > 1 GHz**

**Figure 19. Determination of the reference fields for the high-frequency measurements.**



### 3.1.4 Difficulties with the IEEE 299 Standard

There are a number of difficulties with this standard that preclude it from providing meaningful measurements of the shielding provided by an enclosure. In fact, even the Standard itself recognizes certain difficulties with the requirement:

*The following note should be included with the test data: Electromagnetic SE measurements made at a single frequency in this range may not be representative of measurements made at other frequencies within the range. There may be significant variations due to resonance or other reflective condition effects.*

Furthermore, the Standard recognizes the importance of resonance effects caused by slots or other penetrations. It states:

*There are resonance effects other than cavity resonances that may affect the measured shielding effectiveness of the shielded enclosure. One such phenomenon is slot resonance. The penetration of electromagnetic fields through a given slot in a conducting plane varies with frequency. Slot resonance may occur at frequencies below the fundamental resonance frequency for cavity resonance.*

*These resonance effects are inherent in the electromagnetic performance of the shielded enclosure and are not artifacts of the test technique; consequently, such resonance effects should be considered, as is the case with cavity resonance effects.*

While these statements imply that these cavity resonances should be “considered” in the testing, the Standard states elsewhere that the measurements should try to avoid such resonances. As noted in earlier discussion of the field behavior in resonant cavities (see Figure 12), there can be as much as a 70 dB variation in the shielding effectiveness of a cavity as the frequency varies from resonance (peaks) to anti-resonance (minima). Even if the resonances are all avoided in the measurements, there can be a 35 dB variation in the SE, as it goes from some sort of average value to the anti-resonance values.

Thus, it is logical to also require the avoidance of the anti-resonance frequencies in the SE measurements. This suggests that some other measurement concept that is not sensitive to the cavity resonances should be used to determine the SE of practical cavities. One such measurement approach is suggested later in Section 4 of this report.

In addition to the difficulties posed by the cavity resonances in the IEEE 299 Standard, there are several other difficulties that arise in using this method. These are

1. The definition of the reference field for determining the SE is not consistent. For the low frequency H-field measurements using the loop antennas, and the high frequency ( $f > 1$  GHz) E-field measurements using the horn antennas, the reference fields are truly the *incident fields* produced by the transmitting antenna. However, for the resonance region measurements and the high frequency measurements with  $f < 1$  GHz, the reference fields are the *total fields* (e.g., incident + enclosure-scattered fields). In these latter cases, the reference antenna is located at a position of

maximum response, which very approximately will provide a field response that is a factor of 2 larger than the true incident field. This implies that the shielding effectiveness as measured with this method will be roughly 6 dB too high.

2. For the frequency ranges that require the use of a  $\lambda/2$  dipole antenna, the antenna's length must be adjusted each time the frequency is changed. This precludes any sort of automatic sweeping of the test frequency.
3. The method measures the SE at a very limited number of frequencies. It is impossible to get an adequate understanding of the shielding of the enclosure from such a small sample (see Figure 12.)
4. The measurement procedure requires a manual sweeping of not only the internal receiving antenna, but also the external transmitting antenna. This must be done for each frequency of interest, and consequently, it limits the number of frequencies that can be considered for the testing.
5. The measurement procedure provides magnitude only data, and as such, it is nearly useless in determining transient responses for internal fields or systems.
6. The measurement procedure concentrates many measurements in the vicinity of apertures, cracks or joints in the shield. However, as noted in Figure 11 showing the field pattern in a cavity excited by an aperture, the maximum field is not necessarily located just at the aperture; it can be located throughout the cavity volume, and it depends on the mode structure within the cavity.

## **3.2 MIL-STD-188-125-1**

### *3.2.1 Overview*

MIL-STD-188-125-1 [11] provides information on shielding effectiveness test methods for HEMP purposes. It is similar to the IEEE-STD-299 discussed in the previous section, except that the requirements have been modified to evaluate the barrier performance with a stepped-frequency measurement technique using a minimum set of test areas and test points.

For this test, a transmitting antenna is placed on one side of the electromagnetic barrier on the measurement axis through the center of each test area (or test point). The receiving antenna is centered on the test area (or test point) at the opposite side of the barrier. The instrumentation is then stepped through the measurement frequencies, and the measured data are recorded. Magnetic field shielding effectiveness measurements are made at frequencies from 10 kHz through 20 MHz. Resonant range/plane wave shielding effectiveness is measured from 20 MHz through 1 GHz. Selection of test areas and test points, test frequencies, and polarizations of the transmitting antennas are all defined in this standard.

### *3.2.2 Measurement Concepts*

The measurement concept for this MIL-STD is similar to that of the IEEE measurement. The shielding effectiveness is determined through Eqs.(15) by making a measurement of a suitable reference (incident) field and then a similar measurement of the field within the shielded region. This is done for a number of different frequencies, source locations and polarizations and internal observation points.

#### *3.2.2.1 Measurement Frequencies and Equipment*

Unlike the IEEE 299 Standard, however, there are many more frequencies specified for this MIL-STD test. These frequencies are to be spaced approximately logarithmically within each decade, with minimum sampling density as follows:

- 10kHz – 100kHz – 20 test frequencies
- 100kHz – 1MHz – 20 test frequencies
- 1MHz – 10MHz – 40 test frequencies
- 10MHz – 100MHz – 150 test frequencies
- 100MHz – 16Hz1 – 50 test frequencies

The spacing may be adjusted to avoid discrete system operating frequencies or noise spikes in the ambient electromagnetic environment.

The equipment needed for this MIL-STD-188-125 testing is listed in Table 2, together with the characteristics of these devices. In addition, the required equipment configuration for this testing is shown in Figure 21.

**Table 2. Equipment and characteristics needed for the MIL-STD-188-125 testing.**

Equipment	Characteristics
Oscillators <sup>1</sup>	10 kHz – 1 GHz
Power Amplifiers	10 kHz – 1 GHz; power output as required for dynamic range
Preamplifiers	10 kHz – 1 GHz; amplification and noise figure as required for dynamic range
Receivers, Network Analyzers, or Spectrum Analyzers	10 kHz – 1 GHz
Antenna Kit <sup>2</sup>	10 kHz – 1 GHz
Computer and GPIB Control Interfaces <sup>3</sup>	As required
Fiber Optic (F/O) Links <sup>4</sup>	As required
Miscellaneous Cables, Attenuators, and Coaxial Switches	As required

<sup>1</sup> Oscillators may be integral to the receivers/network or spectrum analyzers, and radio frequency (RF) signals may be transmitted through the shield with an appropriate fiber optic link or high-quality, solid metal-shielded coaxial cable.

<sup>2</sup> Electrostatically shielded loop antennas are required in the low-frequency or magnetic regime (10 kHz - 20 MHz). Biconical antennas shall be used in the resonant frequency range (20 MHz to approximately 100 MHz). Log periodic or equivalent broad band antennas shall be used in the high-frequency or plane wave regime (approximately 100 MHz to 1 GHz). Antennas must radiate and receive over the prescribed frequency bands and, in conjunction with other test equipment, must satisfy the dynamic range requirement.

<sup>3</sup> Use of a personal computer with an IEEE-488 general purpose interface bus (GPIB), or equivalent, to control instrumentation and store test data is strongly recommended.

<sup>4</sup> Use of fiber optic links for transmitting RF or control signals through the shield, as required, is strongly recommended.

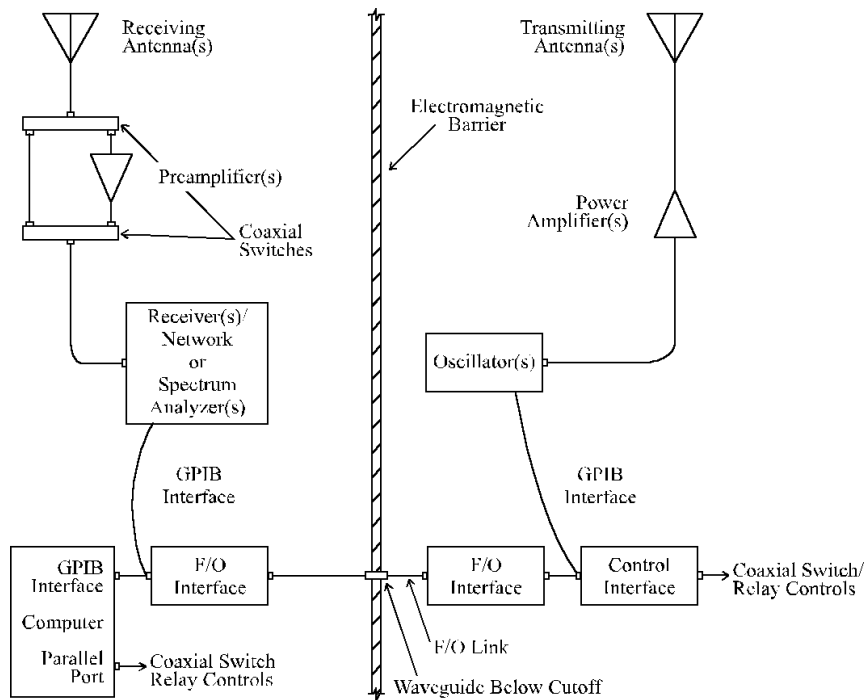


**Figure 21. Equipment configuration for the MIL-STD-188-125 testing.**

### 3.2.2.2 Measured Response Quantities

As noted in Table 2, the measured quantities consist of either the magnetic (H) field at low frequencies, or the electric (E) field at the resonant or plane wave frequency regime. Electrostatically shielded loop antennas are used for the low-frequency measurements in the (10 kHz - 20 MHz range, and biconical antennas are used in the resonant frequency range (20 MHz to approximately 100 MHz). At higher frequencies (approximately 100 MHz to 1 GHz), log periodic or equivalent broadband antennas are used.

As in the IEEE Standard, two measurements must be made: the first is reverence measurement of the incident field from the antenna, and the second is the E or H-field within the enclosure for the same incident field excitation. For the MIL-STD-188-125 testing, the ambiguity of the reference field that is present in the IEEE standard is eliminated. As shown in Figure 22, the determination of the reference field is done by removing the shield and then performing the measurement<sup>4</sup>. Then, the similar measurement is made with the enclosure in place.

In performing the measurements of the internal field in the enclosure, the localized antennas are used to illuminate various portions of the enclosure, as noted in Figure 23. For

<sup>4</sup> In practice, the distance between the two antennas and their heights over the ground are noted, and the antennas are then moved to a distant location where the unimpeded measurement of the field can be made.

both the plane-wave and H-field shielding measurements, the entire surface (including the floor when both sides of the shield are accessible) of the electromagnetic barrier are to be divided into numbered plane areas not greater than 3.05 m x 3.05 m, as illustrated by the example in the figure. The circles in this figure in the center of each area indicate the various transmitting antenna locations required for these measurements.

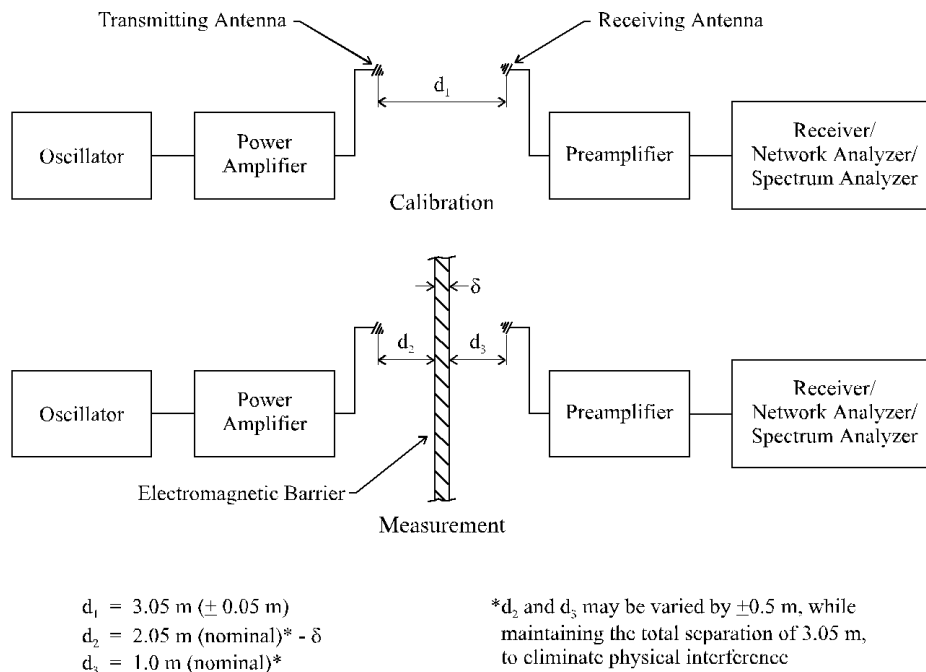


**Figure 22. Relative locations of the transmitting and receiving antennas for calibration and the shielding measurement.**

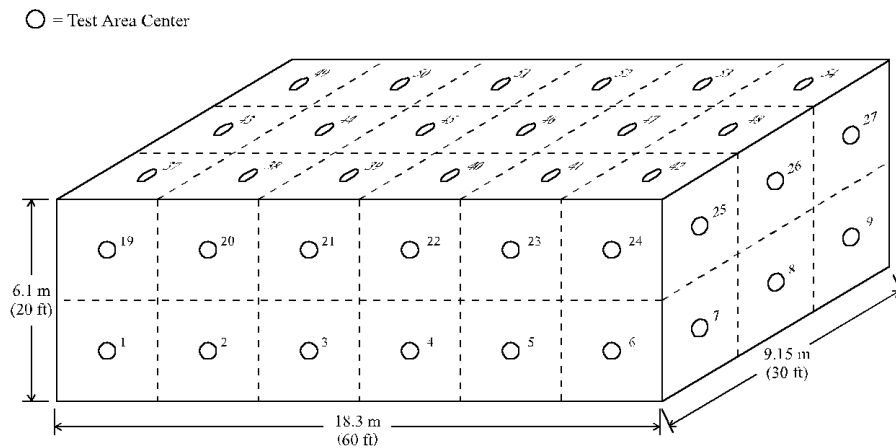


**Figure 23. Example of antenna locations for the localized antenna tests for a hypothetical shielded enclosure or facility**

Unlike the IEEE 299 Standard that requires moving the internal antenna throughout the shielded volume to determine the largest field, the MIL-STD-188-125 uses a fixed test point method. Numbered test points are established at all architectural, mechanical, and electrical points of entry (POEs). The measurement axes for these test points are *normal* to the shield surface at the geometric centers of shielded doors, equipment access panels, and ventilation waveguide-below-cutoff arrays and at the centerlines of penetrating pipes or conduits for piping and electrical POEs.

### 3.2.3 *Measurement Procedures*

According to this standard, the following measurement procedure should be used. Shielding effectiveness measurements for each test area and test point and at each test frequency and required antenna polarization should be performed as shown in Figure 22. Identical equipment, antennas, cables, and equipment settings (except attenuator settings) should be used in the calibration and measurement sequences.

The transmitting antenna should normally be placed outside the electromagnetic barrier, along the measurement axis centered on the test area (or test point). The receiving antenna should normally be inside the barrier and should be centered on the test area (or test point). For the magnetic field measurements, the loops of the transmitting and receiving antennas are to be in the same plane. Dipoles of the transmitting and receiving biconical and log-periodic antennas are located parallel to each other for the resonant range/plane wave measurements. The nominal distance from the transmitting antenna reference point (center of a loop antenna or feed point of a bi-conical or log-periodic antenna) to the test area is 2.05 m (6.7 ft), less the thickness  $\delta$  of the shield. The nominal distance from the receiving antenna reference point to the test area surface is 1 m (3.3 ft), and at least 0.3 m (12.2 in) clearance between the shield and the closest active point on the antenna should be maintained. The transmitting and receiving antenna distances from the shield may be varied by  $\pm 0.5$  m (1.6 ft), while maintaining the total separation of 3.05 m, to eliminate physical interference. The measurement axis may also be displaced from the center of the test area or test point to eliminate physical interference or to maintain the receiving antenna clearance from the shield. These variations and displacements should be noted and recorded.

The instrumentation system should be stepped through the test frequencies, and the received signal strength for each test frequency and antenna polarization should be recorded as the measured signal for that test area (or test point) and configuration. Frequency can be interrupted as necessary to perform antenna and equipment changes.

### 3.2.4 *Difficulties with the MIL-STD-188-125-1 Test*

This test is an improvement over the IEEE 299 Standard, in that the discrepancy in the definition of the reference field is eliminated. In this MIL-STD test, the reference field is the true “incident” field in the absence of the shielded enclosure. In addition, the use of broadband antennas is suggested to eliminate the need for manually adjusting the antenna length to  $\lambda/2$  each time the frequency is changed.

However, several of the deficiencies found in the IEEE testing still remain here. These are:

1. The prescribed method still measures the SE at a limited number of frequencies, and as such, one cannot get an adequate understanding of the overall shielding of the enclosure (see Figure 12.)
2. The measurement procedure requires many external manual transmitting antenna locations. This implies that a tremendous number of measurements will be needed.
3. The measurement procedure still obtains magnitude only data, although the use of a network analyzer would permit, in principle, the determination of phase information. As such, this test method is not useful for determining transient responses for internal fields or systems.
4. The measurement procedure still concentrates the measurements in the vicinity of POEs (apertures, cracks or joints) in the shield. As noted earlier, the field distribution within the enclosure can vary rapidly at all points within the shield.

### **3.3 IEC 61000-4-23**

The International Electrotechnical Commission has developed a third standard dealing with the testing of shielded enclosures. This is the IEC 61000-4-23 standard [12], and it is based primarily in MIL-STD-188-125-1, but with a few modifications: the measurement frequencies in the IEC standard are different, and the IEC standard brings back the sweeping of the internal antenna location and polarization to determine the worst-case response.

Aside from these issues, the IEC 61000-4-23 standard is very close to MIL-STD-188-125-1. Consequently, the IEC standard will not be discussed further here.

### **3.4 MIL-STD-461E**

#### *3.4.1 Overview*

MIL-STD-461E establishes interface and associated verification requirements for the control of the electromagnetic interference (emission and susceptibility) characteristics of electronic, electrical, and electromechanical equipment and subsystems designed or procured for use by activities and agencies of the U.S. Department of Defense. Such equipment and subsystems may be used independently or as an integral part of other subsystems or systems. This standard is designed for items that have the following features: electronic enclosures that are no larger than an equipment rack, electrical interconnections that are discrete wiring harnesses between enclosures, and electrical power input derived from prime power sources.

According to the MIL-STD-461E, this standard should *not* be directly applied to items such as modules located inside electronic enclosures or entire platforms (such as a shielded room or protective enclosure.) Nevertheless, the two portions of this standard that apply to the shielding function of enclosures (equipment boxes with conductors attached), RS101 and RS103, will be briefly summarized for completeness.

#### *3.4.2 RS101 – Magnetic Field Radiated Susceptibility, 30 Hz to 100 kHz.*

The RS101 portion of MIL-STD-461E is applicable to equipment and subsystem enclosures, including electrical cable interfaces. The requirement is not applicable for electromagnetic coupling via antennas. For equipment intended to be installed on Navy aircraft, the requirement is applicable only to aircraft with anti-submarine warfare (ASW) capability. For Army ground equipment, the requirement is applicable only to vehicles having a minesweeping or mine detection capability.

According to this requirement, the equipment under test (EUT) must not exhibit any malfunction, degradation of performance, or deviation from specified indications, beyond the tolerances indicated in the individual equipment or subsystem specification, when subjected to the specified levels of externally-provided magnetic (H) fields, which are provided in the standard. Thus, this test is more of a functional test, rather than a test to quantify the specific shielding levels within an enclosure. For that reason, it has little bearing on the topic of the present report on shielding effectiveness.

### 3.4.3 RS103 – Electric Field Radiated Susceptibility, 2 MHz to 40 GHz.

This requirement is applicable to equipment and subsystem enclosures and all interconnecting cables. The requirement is applicable as follows:

- a. 2 MHz to 30 MHz Army ships; Army aircraft, including flight line; Navy (except aircraft); and optional<sup>5</sup> for all others
- b. 30 MHz to 1GHz all
- c. 1 GHz to 18 GHz all
- d. 18 GHz to 40 GHz optional<sup>2</sup> for all

In the application of this portion of the standard, the EUT must not exhibit any malfunction, degradation of performance, or deviation from specified indications, beyond the tolerances indicated in the individual equipment or subsystem specification, when subjected to the radiated electric fields called-out in the standard. Thus, it too is a functional test of the EUT.

---

<sup>5</sup> Required only if specified in the procurement specification.

#### 4. Recommendations for Testing of Shielded Enclosures

The overall conclusion that can be drawn from the work presented in this note is that the traditional deterministic measurement methods are not practical for electrically large enclosures, where there can be large and unpredictable response variations and significant sensitivity to the electrical configuration. By separating the problem into a deterministic and a statistical component, ref. [9] has suggested one can obtain a simpler and more useful model for the electromagnetic behavior of such enclosures. In their paper, the authors have found that a simple coupling model, combined with a reverberation-chamber-type statistical model, can describe illumination pattern characteristics of the enclosure. The combined model can be used to predict the behavior of a physical, electrically large system.

Drawing upon their work, it appears as if a new type of measurement procedure could be developed for determining the shielding effectiveness of an enclosure. This procedure would be based on the observation that at frequencies above about 6 times the fundamental resonance frequency of the cavity, the resonant modes occur frequently enough in a modest frequency range so that one can assume that they look like a random distribution describable by a mean and standard deviation. Thus, a simple averaging of a measured shielding effectiveness over an appropriately chosen bandwidth would provide an estimate of the mean value of the SE in this range.

Moreover, given the large number of internal cavity modes within the enclosure, it is possible to consider the enclosure itself to be like a mode-stirred chamber, if a suitable rotating blade were installed in the cavity. With such a blade in place, it would be possible to obtain an averaged shielding effectiveness of the enclosure at a single frequency by averaging over all blade positions. As suggested in [9], it would also be possible to consider averaging over the blade position and the frequency, with a subsequent higher level of averaging being performed.

These concepts suggest that the following test procedure for shielding effectiveness may provide useful results for high-frequency excitations.

1. Develop a magnitude/phase measurement system, using the network analyzer as in Figure 21 for the MIL-STD-188-125 testing.
2. Be certain that this measurement system can be swept automatically over a substantial bandwidth without having to manually adjust antennas or cables at each frequency.
3. Determine a reference E-field, using the approach shown in Figure 22 (top).
4. Install within the chamber a motorized blade that rotates and stirs the internal modes.
5. With the internal antenna and the blade installed in the facility (as in Figure 22 (bottom)), perform the shielding effectiveness measurements. For these measurements, the approach used in ref. [9] is possible. As

described in their report, the network analyzer was set to scan 801 points over a very narrow frequency span (100 Hz) in approximately 0.8 seconds, which was the rotation period of the turning paddle. Since the frequency span was so narrow, the resulting trace was essentially a plot of received power versus time, or equivalently, the received power versus relative paddle position. Different sweeps can be taken at different starting frequencies and the recorded data averaged at each frequency, and perhaps averaged over a narrow frequency band. This will provide an average SE for the specific choice of illumination and observation point parameters.

6. These measurements should then be repeated for different observation points and illumination.

It is recommended that such a test concept for the measuring of the SE of an enclosure be examined more closely to see if it will provide a reasonable alternative to the IEEE and MIL-STD tests that are currently in use.

## 5. References

1. Tesche, F. M., "Summary and Comparison of HEMP Standards for Testing and Protection", Report prepared for the Swiss Defense Procurement Agency of the Federal Department of Defense, Civil Protection and Sports, December 6, 1999. A copy of this can be obtained from the second author (DVG) by e-mailing him at Giri@DVGiri.com
2. Tai, C. T., and P. Rozenfeld, "Different Representations of Dyadic Green's Functions for a Rectangular Cavity", **IEEE Trans. MTT**, Vol MTT-24, No. 6, September 1976.
3. Rahmat-Samii, Y., "On the Question of Computation of the Dyadic Green's Function at the Source Region in Waveguides and Cavities", **IEEE Trans. MTT**, Vol MTT-23, September 1975.
4. Wu, D., and D. C. Chang, "An Investigation of a Ray-Mode Representation of the Green's Function in a Rectangular Cavity", NBS Technical Note 1312, U.S. National Bureau of Standards, September, 1987.
5. Ramo, S., J. R. Whinnery, & T. Van Duser, **Fields and Waves in Communication Electronics**, Second Edition. John Wiley and Sons, 1989.
6. Collin, R. E., **Field Theory of Guided Waves**, McGraw Hill, New York, 1960
7. Siah, E. S., K. Sertel, J. L. Volakis and V. Liepa, "EM Coupling and Suppression through Slots into Lossless Overmoded Cavities using the Multilevel Fast Multipole Algorithm", Digest of the 2002 IEEE EMC Symposium, Minneapolis, MN, August, 2002, pp 161-166.
8. Bunting, C. F., and Shih-Pin Yu, "Statistical Shielding Effectiveness – an Examination of the Field Penetration in a Rectangular Box using Modal MOM", Digest of the 2002 IEEE EMC Symposium, Minneapolis, MN, August, 2002, pp 211-215.
9. Ladbury J. M., T. H. Lehman, and G. H. Koepke, "Coupling to Devices in Electrically Large Cavities, or Why Classical EMC Evaluation Techniques are Becoming Obsolete", Digest of the 2002 IEEE EMC Symposium, Minneapolis, MN, August, 2002, pp 648-655.
10. "IEEE Standard Method for Measuring the Effectiveness of Electromagnetic Shielding Enclosures", IEEE Std 299-1997 (Revision of IEEE Std 299-1991), Approved 9 December 1997, IEEE Standards Board.
11. "High-Altitude Electromagnetic Pulse (HEMP) Protection for Ground-Based C<sup>4</sup>I Facilities Performing Critical, Time-Urgent Missions: Part 1 – Fixed Facilities", U.S. Department of Defense Interface Standard, MIL-STD-188-125-1, 17 July 1998.

12. IEC 61000-4-23, Electromagnetic Compatibility (EMC) – Part 4-23: Testing and Measurement Techniques - Test Methods for Protective Devices for HEMP and Other Radiated Disturbances, Basic EMC Publication, 2000.